Free-energy coupling of nanoparticles and liquid crystal from molecular simulation of the isotropic-nematic transition

E-mail:

30 September 2022

Abstract. Dynamical models of nanoparticle assembly guided by liquid crystals require as input mean-field models for the free energy of nanoparticle-mesogen mixtures. Current microscopic theory offers limited guidance for modeling the coupling parameter g between particle concentration and nematic order parameter. We used molecular dynamics simulations of rigid chains of Lennard-Jones segments and larger LJ nanoparticles to determine g from shifts in the isotropic-nematic transition temperature. We found good agreement between our simulations, a Landau-de Gennes free energy model and available experimental data for transition temperature shifts in 8CB mixed with nanoscale dopants (biphenyl and cyclohexane), and estimated that $g = 53$ MPa at standard pressure. We also found that g increases as the fourth power of pressure and that the entropy change across the isotropic-nematic transition is independent of pressure, but increases linearly with the volume of individual nanoparticles. The latter result is useful to predict the latent heat of the transition for this type of mixtures. Therefore, molecular dynamics simulations with improved detail are expected to be very well suited to provide accurate information regarding the coupling parameter g of nanoparticle-mesogen mixtures, especially if advanced simulation methods originally developed for determination of chemical potentials are adapted for this purpose.

Keywords: Nanoparticles, liquid crystal, transition temperature, mean field free energy, coupling parameter, molecular simulation.

1. Introduction

Nanocomposites, whether occurring in nature or designed for technological applications, remain the focus of intense research, both for fundamental scientific reasons as well as due to their potential for achieving desirable properties in new materials. For instance, nanocomposites featuring nanoparticles dispersed in a liquid crystal medium [1, 2] have opened new directions for tuning the properties of the host liquid crystal [3], applications in photonics [4], energy conversion [5], chemical and biological sensing [6]. Another important example of nanocomposites are those involving assembly of nanoparticle structures with well-defined shape and size. As examples of the latter, we can mention blue-phase liquid crystals, able to sort and organize nanoparticles into their highly ordered lattices of topological defects [7], as well as Ghosh, Hirst and co-workers' experiments demonstrating formation of micron-sized nanoparticle structures by partition away from nematic domains and into locally isotropic regions [8, 9, 10].

The most common nanoparticle dopants used in liquid crystals belong to a few primary groups: ferromagnetic [11], ferroelectric [12], metal, semi-conductor and carbon nanoparticles [4]. To stabilize the dispersion of such dopants in the LC host, nanoparticle modification with DNA, proteins, or nematogenic moieties is essential [1, 5]. The composite materials' properties depend subtly on the dopant's size and specific chemistry, as well as preparation conditions and time [4, 10]. While this opens up exciting opportunities for tailoring the physical properties of a given blend, hence avoiding *de novo* synthesis of specialized molecules, it also shows that developing a basic understanding of the structure and properties of nanoparticle-liquid crystal composites is a major outstanding challenge for applications.

Nevertheless, performing the required experiments is very difficult in many cases, while guidance from current microscopic theory is quite limited [2]. Therefore, when studying the thermodynamics of nanoscaled dopants mixed with mesogens, it is reasonable to start from a free energy model that involves the nematic order parameter S and the nanoparticle volume fraction η, including a term that couples them [13, 14]:

$$f = \frac{a(T - T^*)}{2} S^2 - \frac{w}{3} S^3 + \frac{u}{4} S^4 + B\eta^2 + \frac{g}{2} \eta S^2. \tag{1}$$

The phenomenological parameters a, T^*, w and u of the Landau-de Gennes expansion in (1) can be computed from measurable properties of the nematic-isotropic transition [15], while B is a second virial coefficient for the NPs.

However, theoretical calculation of g from microscopic information is not as straightforward. An early approach for determining a coupling parameter similar to g was advanced by Elder et al. [16]; they expanded the Bragg-Williams free energy for a binary alloy to obtain an expression for their coupling parameter. However, that expression requires in turn knowledge of Young's modulus, number densities for each species, the relation between the lattice parameter and alloy composition, and atomic interaction strengths.

From thermodynamics, g can be measured from the relationship between the clearing-point temperature and nanoparticle volume fraction, as follows: A non-zero coupling coefficient g implies a shift in the nematic-isotropic transition, proportional to the nanoparticle volume fraction [13]:

$$T_{IN}(\eta) = T_{IN}^0 - \frac{g}{a}\eta, \tag{2}$$

where T_{IN}^0 is the clearing point for the pure nematic. A downward shift in T_{IN} with increasing η has been observed experimentally both for non-mesogenic molecules, such as cyclohexane and biphenyl [13], and for dilute CdSe [17] and $BaTiO_3$ [18] nanoparticles, but no determination of g was reported.

Still another possible approach is obtaining the necessary information about the function $T_{IN}(\eta)$ from molecular simulations instead of from experiments. Recent simulations of rigid linear chains of Lennard-Jones segments have shown that nematic phases can be obtained if such chains have six or more segments [19]. Moreover, very rigid chains of repulsive Lennard-Jones segments have been used to represent a low-molecular weight mesogen (6CB) interacting with nonmesogenic cyclohexane or water [20]. These simulations identified distinct behavior for miscible and non-miscible dopants (clearing-point temperature depression for cyclohexane and phase separation for water, respectively).

The aim of this work, therefore, is to ascertain whether molecular simulations can be used effectively to determine the coupling parameter g in mixtures of nanoparticles and mesogens, by measuring the small shifts in clearing-point temperatures associated with increasing NP volume fraction.

In what follows, we describe molecular dynamics simulations of a mixture of rigid linear LJ chains and LJ nanospheres, examining the mixture's thermodynamic properties as the nanoparticle volume fraction η is systematically increased: shifts in the transition temperature T_{IN}, the jump in order parameter across the transition ΔS_{IN}, and the phase-change enthalpy Δh_{IN} and entropy Δs_{IN}.

We determined that these changes, observed in our molecular dynamics simulations, are consistent with a free-energy coupling term given by $g\eta S^2/2$. Moreover, we found that the coupling coefficient g is positive and highly pressure-dependent.

Since g is determined from thermodynamic relations, our method can provide independent input for the dynamical equations of the nematization and nanoparticle concentration fields [14], paving the way for prediction of the segregation dynamics that occur during self-assembly of nanoparticles by liquid-crystal sorting [10] (instead of fitting parameters to it). Also, because the coupling term was observed to be linear in η, we propose alternative single-nanoparticle simulation methods (based on chemical potential measurements for a nanoparticle in the nematic phase) that may be more efficient for the calculation of the coupling coefficient g.

2. Methods

In our simulations of mixtures of mesogens and nanoparticles, mesogens are represented with rigid linear chains of nine spherical Lennard-Jones segments. The Lennard-Jones parameters of energy and length for intermolecular interaction among these segments are ϵ_m and σ_m, respectively. They were used to define reduced variables for temperature, pressure and time:

$$T^* = k_B T/\epsilon_m, \tag{3}$$

$$P^* = P\sigma_m^3/\epsilon_m, \tag{4}$$

$$t^* = t\sqrt{\frac{\epsilon_m}{m\,\sigma_m^2}}, \tag{5}$$

where m is the mass of a single LJ segment in the mesogens. The nanoparticles are represented by a single Lennard-Jones sphere. The LJ interaction energy between nanoparticles was set to the same value as mesogen segments,

$$\epsilon_n = \epsilon_m, \tag{6}$$

but the nanoparticle's LJ size parameter σ_n was varied so that their reduced diameter $\sigma_n^* = \sigma_n/\sigma_m = 2$, 4 and 5. We used Lorentz-Berthelot combination rules for the energy and size parameters of the interaction between nanoparticles and mesogen segments:

$$\epsilon_{nm} = (\epsilon_n\epsilon_m)^{1/2}, \tag{7}$$

$$\sigma_{nm} = \frac{\sigma_n + \sigma_m}{2}. \tag{8}$$

We performed molecular dynamics in the isothermal-isobaric ensemble using the HOOMD-blue software, version 2.9.0 [21]. The constant pressure and temperature conditions are achieved in HOOMD-blue with a Martyna-Tobias-Klein barostat-thermostat [22, 23]. Adequate pressure and temperature ranges for observing the isotropic-nematic transition were estimated by interpolating simulation data for rigid linear LJ chains with 8 and 10 segments reported by Oyarzún-Rivera et al. [19]. The number of particles for each species in the mixture was fixed at $N_m = 1000$ for mesogens and, since we wanted to simulate nanoparticles at dilute conditions, $N_n = 4$ for nanoparticles.

In reduced units, the simulations had a time step $\delta t^* = 0.005$. After an equilibration stage with typical duration $t^*_{\text{eq}} = 2.5 \cdot 10^4$, we sampled the system configurations in equilibrium for a duration $t^*_{\text{sam}} = 10^5$.

The HOOMD-blue software directly samples the temperature, pressure, and volume of the periodic simulation cell, but not the nematization order parameter S. To obtain the nematization, for each simulation we periodically sampled the individual mesogen orientations and computed the instantaneous alignment tensor

$$\mathbf{Q}(t) = \langle \mathbf{u}_i(t)\mathbf{u}_i(t) - \mathbf{I}/3 \rangle_i \,, \tag{9}$$

where $\mathbf{u}_i(t)$ is a unit vector indicating the orientation of mesogen i at time t, $\mathbf{I}$ is the identity tensor and the brackets indicate an average with the index i running over all

the linear chains. Then, the nematization order parameter was calculated as

$$S = \frac{2}{3} \langle \lambda_1(t) \rangle_t \,, \tag{10}$$

where $\lambda_1(t)$ denotes the largest eigenvalue of $\mathbf{Q}(t)$ and the angular brackets denote time averaging over the sampling period. We determined the nanoparticles' volume fraction at each state as

$$\eta = \frac{\pi}{6} \rho_n \sigma_{22}^3, \tag{11}$$

where

$$\rho_n = \frac{N_n}{\langle V \rangle} \tag{12}$$

is the nanoparticle number density and $\langle V \rangle$ is the mean volume for the corresponding simulation.

For pure mesogens and each mixture with nanoparticles of fixed size, we determined the isotropic-nematic phase transition temperature $T^*_{IN}(P^*)$, along a given isobar by fitting the nematization S as a function of temperature T^*. The fitting function was of hyperbolic tangent form:

$$S(T^*) = \frac{S_N - S_I}{2} \tanh\left(\frac{T^*_{IN} - T^*}{\delta T^*}\right) + \frac{S_N + S_I}{2}, \tag{13}$$

with parameters S_N and S_I for the values of the order parameter on the nematic and isotropic phases, T^*_{IN} for the reduced transition temperature, and δT^* for the width of the hyperbolic fit. Parameters S_I and δT^* are not zero due to the finite size of the simulated system. The system volume V^* was also fitted as a function of reduced temperature for each isobar and mixture with nanoparticles of fixed size. The fitting function was also of hyperbolic tangent form, but with an additional term linear in T^*,

$$V^*(T^*) = \frac{V^*_N - V^*_I}{2} \tanh\left(\frac{T^*_{IN} - T^*}{\delta V^*}\right) \tag{14}$$

$$+ \frac{V^*_N + V^*_I}{2} + A\, T^*, \tag{15}$$

with parameters V^*_N and V^*_I for the system volume at either side of the transition, δV^* for the width of the hyperbolic fit, and parameter A allowing for volumetric thermal expansion.

As stated before, for each isobar we expected a linear relation between the phase transition temperature T^*_{IN} and the nanoparticle volume fraction η, so we performed least-squares regression of our results to the following form:

$$T^*_{IN} = T^*_{IN,0} - g^*\, \eta, \tag{16}$$

where the intercept $T^*_{IN,0}$ stands for the transition temperature for a pure mesogen at the given pressure and the negative of the slope g^* is a reduced free-energy coupling parameter, as obtained from (2).

In addition, we obtained the entropy and enthalpy changes associated with the isotropic-nematic transition by the following procedure: for a mixture with n species

involving equilibrium between phases α and β, we represent the mixture composition in phase α as the vector $\mathbf{x}^{(\alpha)} = (x_1, \ldots, x_n)$. Then, the composition change $\mathrm{d}\mathbf{x}^{(\alpha)}$ in phase α, associated with changes in the transition temperature and pressure, are related to the molar Gibbs free energy $\hat{G}^{(\alpha)}$, molar volume $\hat{V}^{(\alpha)}$ and molar entropy $\hat{S}^{(\alpha)}$ in phase α by [24]

$$\begin{aligned}
&\left(\mathbf{x}^{(\beta)} - \mathbf{x}^{(\alpha)}\right) \hat{G}^{(\alpha)} \mathrm{d}\mathbf{x}^{(\alpha)} = \\
&\left[\hat{S}^{(\alpha)} - \hat{S}^{(\beta)} + \left(\mathbf{x}^{(\beta)} - \mathbf{x}^{(\alpha)}\right) \nabla \hat{S}^{(\alpha)}\right] dT \\
&- \left[\hat{V}^{(\alpha)} - \hat{V}^{(\beta)} + \left(\mathbf{x}^{(\beta)} - \mathbf{x}^{(\alpha)}\right) \nabla \hat{V}^{(\alpha)}\right] dP,
\end{aligned} \tag{17}$$

where $\nabla \hat{S}^{(\alpha)}$ and $\nabla \hat{V}^{(\alpha)}$ are the gradients of the molar entropy and molar volume with respect to compositions. When applied to our simulations, performed at constant composition, the coefficients $\left(\mathbf{x}^{(\beta)} - \mathbf{x}^{(\alpha)}\right)$ are zero and (17) becomes equivalent to the Clapeyron equation,

$$\left[\hat{S}^{(\alpha)} - \hat{S}^{(\beta)} +\right] dT - \left[\hat{V}^{(\alpha)} - \hat{V}^{(\beta)}\right] dP = 0, \tag{18}$$

which can also be expressed in terms of per-particle quantities instead of molar ones.

For our analysis, we denote the per-particle value w^* of an extensive quantity W^* by the quotient

$$w^* = \frac{W^*}{N_m + N_n}. \tag{19}$$

Since the per-particle entropy and enthalpy changes across the I-N transitions are related by

$$\Delta s^* = \Delta h^* / T^*_{IN}, \tag{20}$$

we calculated the per-particle entalphy change Δh^* for the I-N transition (that is, its latent heat) from the Clapeyron equation,

$$\frac{dP^*}{dT^*_{IN}} = \frac{\Delta h^*}{T^*_{IN}(v^*_I - v^*_N)}, \tag{21}$$

where v^*_I and v^*_N are the reduced volumes per particle of the isotropic and nematic phases, respectively. Instead of estimating the derivative dP^*/dT^*_{IN} from finite differences, we fitted the transition temperature as a function of pressure (for each isobar and mixture) and calculated the required derivative from the reciprocal of dT^*_{IN}/dP^* from that fit. The corresponding per-particle entropy change was obtained finally from (20).

3. Results

We analyzed our simulation data for each isobar and each particle size by plotting the nematization S (the nematic order parameter) as a function of reduced temperature T^* (see figure 1a and table 1 in the Appendix). As expected, the nematization decreases sharply as the system changes from the nematic phase (figure 1b) to the isotropic one (figure 1c).

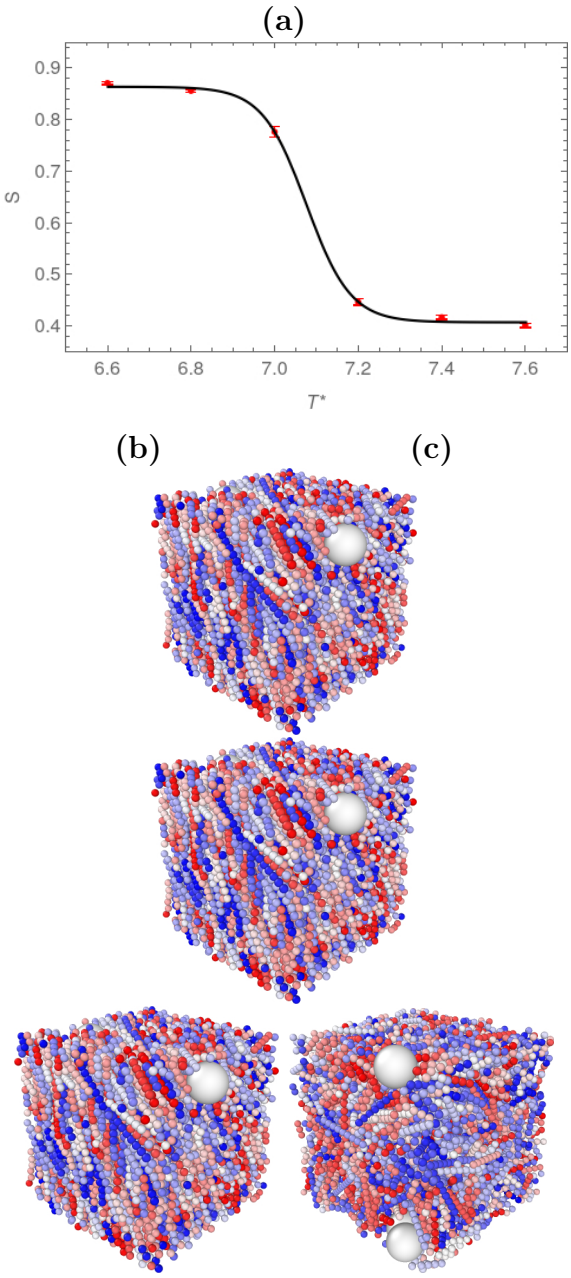

Figure 1. Molecular dynamics of a mixture of nanoparticles and rigid linear chains of nine Lennard-Jones monomers indicate (a) a swift decrease of the nematization order parameter S as a function of reduced temperature T^* at constant pressure; the solid line is a fit to (13). This corresponds to a phase transition between (**b**) a nematic phase and (**c**) an isotropic phase. The transition occurs at a temperature T^*_{IN} that is quite sensitive to pressure. Results in this figure correspond to $P^* = 1.8$.

We determined the transition temperature T^*_{IN} for each isobar by fitting the nematization with a hyperbolic tangent function of temperature. The solid line in figure 1a illustrates this, while table 2 in the Appendix gives the results for all simulated isobars. We also obtained the nematization difference ΔS across the phase transition

from these fits (see table 3, also in the Appendix).

Since our simulations are performed at constant N, P and T, we determined the nanoparticle volume fraction at the phase transition temperature from a hyperbolic-tangent fit of the average volume for each isobar (see table 4 in the Appendix). This allowed us to plot T^*_{IN} as a function of η, see figure 2. The transition temperature did decrease linearly with the nanoparticle packing fraction, but the intercept and slope vary noticeably with pressure. We obtained the values of the intercept $T^*_{IN,0}$ and reduced coupling parameter g^* for each isobar by linear regression; the lines in figure 2 correspond to such fits, while table 5 in the Appendix lists the regression parameters.

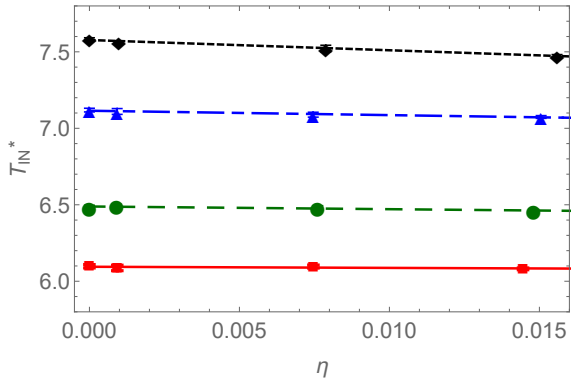

Figure 2. At constant pressure, the isotropic-nematic transition temperature T^*_{IN} decreases linearly with increasing nanoparticle volume fraction η, as shown for the four isobars $P^* = 1.3$ (red squares and solid line), 1.5 (green circles and dashed line), 1.8 (blue triangles and long-short-dashed line) and 2.3 (black diamonds and dotted line); error bars are smaller than the symbol size. Parameter g, which couples η to the nematization S in the free energy of the system, can be determined from the slope of each of these isobars.

Figure 3 shows that the coupling parameter g^* is indeed positive and increases rapidly with increasing pressure. This means that dispersion of nanoparticles is hindered in the nematic phase, and it becomes more unfavorable as pressure rises. This confirms that the assumption of positive coupling parameter is appropriate in continuum-based dynamic equations for the evolution of nanoparticle concentration and nematic order parameter in nanoparticle-mesogen mixtures, such as those in [14].

As our final results, we computed the per-particle enthalpy change Δh^* and entropy change Δs^* of the isotropic-nematic transition from the Clapeyron equation. Figure 4 shows that the latent heat increases linearly with pressure (see also table 6 in the Appendix).

The associated entropy change Δs^* turned out to be independent of pressure and proportional to nanoparticle volume, as shown in figure 5 (also see table 7 in the Appendix).

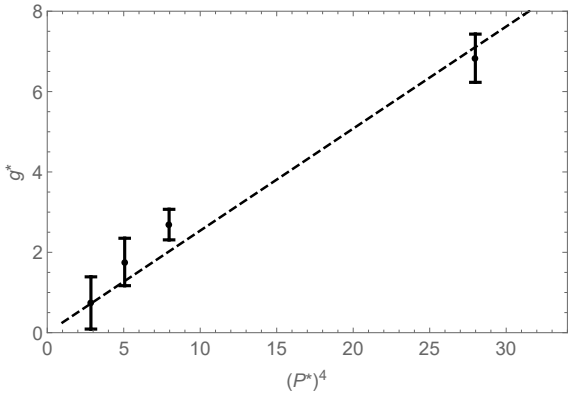

Figure 3. The free-energy coupling parameter g^* is positive and increases rapidly with the fourth power of the pressure P^*. Thermodynamically, this means that dispersion of nanoparticles in the nematic phase becomes rapidly more unfavorable as pressure is increased.

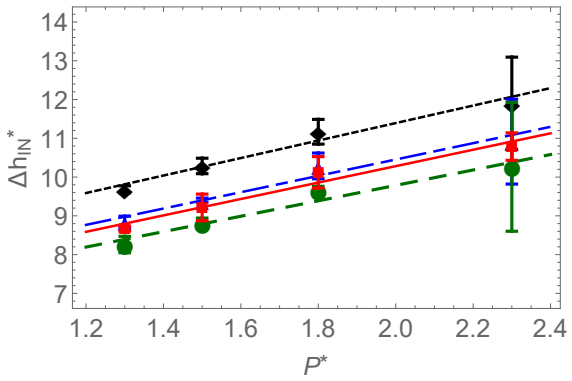

Figure 4. The latent heat per particle Δh^*_{IN} associated with the isotropic-nematic transition, computed from (21), increases linearly with pressure for the pure mesogen system (red squares and solid line) and each nanoparticle diameter $\sigma^*_n = 2$ (green circles and dashed line), 4 (blue triangles and long-short-dashed line) and 5 (black diamonds and dotted line). The lines correspond to linear regression fits.

4. Discussion

As considered in the introduction, the change in nematization ΔS associated with the isotropic-nematic transition is independent of η for a free-energy coupling between the nanoparticle volume fraction and the square of the nematization order parameter. On the other hand, the nematization change ΔS would increase with η for a coupling linear in S. Our results for the rigid linear LJ chains mixed with LJ nanoparticles are consistent with the former type of free-energy coupling, but not with the latter. This is relevant for continuum-based dynamic theories that rely on modeling the free energy density of mesogens and nanoparticles to study their time evolution. These theories also require knowledge about the magnitude of the coupling parameter g.

In our simulations, we observed a percent reduction in the I-N transition

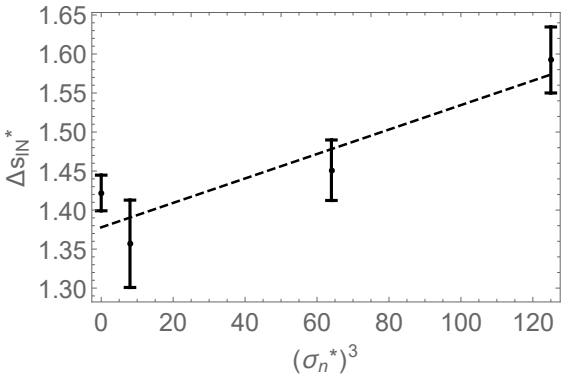

Figure 5. The per-particle entropy change Δs^*_{IN} associated to the isotropic-nematic transition, computed from (19), is independent of pressure but is proportional to $(\sigma^*_n)^3$ and, therefore, to nanoparticle volume. The dashed line corresponds to a linear regression fit.

temperature of -1.4% for $\eta = 0.016$. We can compare this value with the results from Denolf et al. for 8CB doped with a molar fraction of biphenyl in the range $0 \leq x_{BP} \leq 0.16$ of biphenyl or with a molar fraction of cyclohexane $0 \leq x_{CH} \leq 0.09$ [13]. Taking into account the molar masses and densities of biphenyl, cyclohexane and 8CB [25, 26], we estimated that $\eta = 0.016$ corresponds to a biphenyl molar fraction x_{BP}= 0.031 and a cyclohexane molar fraction x_{CH}= 0.042. The corresponding percent reductions in the I-N transition temperature, obtained by interpolation of the results of Denolf et al., are -1.1% for biphenyl and -1.5% for cyclohexane; the agreement between simulations and experiments is therefore quite good.

The free energy model given by (1) also predicts an entropy-density change for the isotropic-nematic phase transition that depends solely on parameters a, w and u [13],

$$\frac{\Delta S_{IN}}{V} = \frac{2aw^2}{9u^2}. \tag{22}$$

In our simulations, we found a per-particle entropy change Δs^* that is independent of pressure, but increases linearly with the NP volume. One way to understand this result is positing that such entropy is associated mostly with the mesogens, but that larger NPs perturb them more strongly.

Using the free energy (1), we can calculate the coupling parameter g that matches a relative reduction $R = T_{IN}/T_{IN,0} - 1$ in the transition temperature: from (2),

$$g = -R\frac{aT_{IN,0}}{\eta}. \tag{23}$$

From our results for R and η, using the values $a = 190$ kPa/K [27, 28] and $T_{IN,0} = 313.8$ K for 8CB [29], we find $g = 53$ MPa. Here must point out that our simulations indicate that the value of g is quite sensitive to pressure changes.

The linear dependence with η that we observed for the depression of the isotropic-nematic transition temperature also indicates that a single-particle theoretical description could be adequate to interpret the associated free energy coupling term;

that is, we could measure with simulations the effect of a single nanoparticle interacting with the mesogen fluid and then scale it by the nanoparticle volume fraction. One approach for doing this could be interpreting g in terms of the chemical potential, which corresponds to the derivative of the free energy density with respect to nanoparticle density,

$$\mu_n = \left(\frac{\partial f}{\partial \rho_n}\right)_{N_m,T,P} \tag{24}$$

$$= \mu_{n,0} + g\frac{S^2}{2}, \tag{25}$$

where $\mu_{n,0}$ corresponds to the chemical potential of nanoparticles in the fully disordered isotropic phase. Hence, if one measures the chemical potential of nanoparticles in a nematic phase (as a function of increasing nematization) that would allow direct calculation of the coupling parameter g. This procedure is hindered by the fact that both the isotropic and nematic phases are relatively dense. Thus, simple particle-insertion schemes such as Widom's particle insertion method [30] or Benett's insertion-removal method [31] for computing chemical potentials may be inefficient and inadequate for this problem. Nevertheless, more advanced simulations schemes such as metadynamics [32], chemical potential perturbation [33] or adaptive resolution simulations [34]), among others, may be useful for directly measuring the free-energy coupling parameter g.

The strong dependence of g on P may lead to formation of spatially-periodic NP structures due to standing acoustic waves or passing shockwaves. In addition, this pressure-dependence could also be exploited by varying pressure, and therefore system behavior, non-periodically. For instance, this could be achieved experimentally by using centrifugation to vary the effective hydrostatic pressure, or by rapidly-moving solids, such as propellers or granular particles, through the system, producing local pressure variations by essentially the same mechanisms responsible for phenomena such as cavitation. Likewise, our results raise the question of whether active nanoparticles could also be used to produce local pressure variations and give rise to new structure-forming effects and, of course, of how to optimally study this with molecular dynamics simulations.

5. Acknowledgments

6. Appendix

Tables 1 to 7 detail the numerical results from our simulations and analysis.

Table 1. Nematic order parameter S of pure mesogens and mixtures of the given nanoparticle diameter σ_n^*, for the given values of the reduced pressure P^* and temperature T^*.

P^*	T^*	Pure	$\sigma_n^* = 2$	$\sigma_n^* = 4$	$\sigma_n^* = 5$
1.3	5.6	0.9168(15)	0.9069(24)	0.9129(15)	0.9032(15)
	5.8	0.8944(19)	0.8678(40)	0.8830(21)	0.8892(33)
	6.0	0.8536(26)	0.8285(50)	0.8170(32)	0.8120(04)
	6.2	0.4359(50)	0.4306(70)	0.4385(60)	0.4147(50)
	6.4	0.3965(50)	0.3965(60)	0.3664(40)	0.3766(40)
	6.6	0.3807(40)	0.3554(60)	0.3599(40)	0.3676(40)
6.4 1.5	6.0	0.9004(16)	0.8902(19)	0.8846(23)	0.8932(19)
	6.2	0.8732(26)	0.8671(27)	0.8625(24)	0.8812(29)
	6.4	0.8286(33)	0.8321(32)	0.8273(32)	0.7983(40)
	6.6	0.4131(60)	0.4137(50)	0.4004(50)	0.3919(60)
	6.8	0.3799(60)	0.3797(40)	0.3850(50)	0.3863(40)
	7.0	0.3954(50)	0.3834(40)	0.3834(40)	0.3834(40)
1.8	6.6	0.8917(20)	0.8609(24)	0.8694(80)	0.8706(27)
	6.8	0.8616(24)	0.8556(40)	0.8355(28)	0.8557(28)
	7.0	0.8199(40)	0.8262(60)	0.7257(40)	0.776(11)
	7.2	0.4858(60)	0.4417(40)	0.4827(60)	0.4461(60)
	7.4	0.3944(40)	0.3785(50)	0.4058(40)	0.4164(40)
	7.6	0.3780(50)	0.3557(43)	0.3612(40)	0.4011(40)
2.3	7.0	0.9132(28)	0.8911(23)	0.8862(33)	0.8862(33
	7.2	0.8944(28)	0.8846(22)	0.8760(26)	0.8885(23)
	7.4	0.8606(40)	0.8736(40)	0.8407(40)	0.7530(70)
	7.6	0.6049(70)	0.5429(70)	0.4799(60)	0.4736(60)
	7.8	0.3891(40)	0.3901(50)	0.4218(40)	0.3991(40)
	8.0	0.3889(50)	0.3650(40)	0.3686(40)	0.3856(40)

Table 2. Isotropic-nematic transition temperature T_c^* of pure mesogens and mixtures of the given nanoparticle diameter σ_n^*, for the given pressure P^*.

P^*	Pure	$\sigma_n^* = 2$	$\sigma_n^* = 4$	$\sigma_n^* = 5$
1.3	6.098(11)	6.087(18)	6.096(10)	6.081(06)
1.5	6.482(15)	6.492(11)	6.480(14)	6.460(10)
1.8	7.119(12)	7.110(19)	7.089(16)	7.074(09)
2.3	7.585(07)	7.564(08)	7.521(22)	7.475(07)

Table 3. Change of the nematization $\Delta S = S_N - S_I$, across the isotropic-nematic transition, of pure mesogens and mixtures of the given nanoparticle diameter σ_n^*, for the given pressure P^*.

P^*	Pure	$\sigma_n^* = 2$	$\sigma_n^* = 4$	$\sigma_n^* = 5$
1.3	0.6471(67)	0.6418(97)	0.6307(70)	0.6344(37)
1.5	0.6369(75)	0.6302(58)	0.6289(55)	0.6333(43)
1.8	0.6310(78)	0.624(12)	0.6161(87)	0.6363(48)
2.3	0.6403(78)	0.6321(54)	0.638(13)	0.6414(45)

Table 4. Nanoparticle volume fraction η at the isotropic-nematic transition of pure mesogens and mixtures of the given nanoparticle diameter σ_n^*, for the given pressure P^*.

P^*	Pure	$\sigma_n^* = 2$	$\sigma_n^* = 4$	$\sigma_n^* = 5$
1.3	0.000	0.000929(2)	0.007467(1)	0.014455(2)
1.5	0.000	0.000904(1)	0.007613(1)	0.014813(2)
1.8	0.000	0.000925(7)	0.007461(1)	0.015058(2)
2.3	0.000	0.000980(2)	0.007880(2)	0.015588(2)

Table 5. Reduced coupling parameter g^* and pure-mesogen transition temperature $T_{c,0}^*$, from linear regression of the isotropic-nematic transition temperature in terms of the nanoparticle volume fraction, for the given pressure P^*.

P^*	g^*	$T_{c,0}^*$
1.3	0.74(65)	6.095(5)
1.5	1.76(59)	6.489(5)
1.8	2.69(38)	7.115(3)
2.3	6.83(60)	7.577(5)

Table 6. Latent heat per particle Δh^* for the isotropic-nematic transition of pure mesogens and mixtures with given nanoparticle diameter σ_n^*, for the given pressure P^*.

P^*	Pure	$\sigma_n^* = 2$	$\sigma_n^* = 3$	$\sigma_n^* = 5$
1.3	8.67(07)	8.26(21)	8.85(15)	9.68(09)
1.5	9.22(34)	8.81(13)	9.40(05)	10.29(20)
1.8	10.12(40)	9.65(11)	10.29(33)	11.17(32)
2.3	10.79(35)	10.3(17)	10.9(11)	11.9(12)

Table 7. Per-particle entropy change Δs^* for the isotropic-nematic transition of pure mesogens and mixtures with given nanoparticle diameter σ_n^*, for the given pressure P^*.

P^*	Pure	$\sigma_n^* = 2$	$\sigma_n^* = 3$	$\sigma_n^* = 5$
1.3	1.42(01)	1.36(04)	1.45(02)	1.59(02)
1.5	1.42(05)	1.36(02)	1.45(01)	1.59(03)
1.8	1.42(06)	1.36(02)	1.45(05)	1.59(05)
2.3	1.42(05)	1.36(22)	1.45(15)	1.59(16)

7. References

[1] Hegmann T, Qi H and Marx V 2007 *Journal of Inorganic and Organometallic Polymers and Materials* **17** 483–508

[2] Singh S 2019 *Crystals* **9** 475

[3] Shao B, Wan S, Yang C, Shen J, Li Y, You H, Chen D, Fan C, Liu K and Zhang H 2020 *Angewandte Chemie International Edition* **59** 18213–18217

[4] Shen Y and Dierking I 2019 *Applied Sciences* **9** 2512

[5] Lagerwall J P and Scalia G 2012 *Current Applied Physics* **12** 1387–1412

[6] Joshi A, Manjuladevi V, Gupta R K and Kumar S 2020 *Nanotechnology* **31** 365605

[7] Stratford K, Henrich O, Lintuvuori J S, Cates M E and Marenduzzo D 2014 *Nature Communications* **5** 3954

[8] Rodarte A L, Cao B H, Panesar H, Pandolfi R J, Quint M, Edwards L, Ghosh S, Hein J E and Hirst L S 2015 *Soft Matter* **11** 1701–1707

[9] Atzin N, Guzmán O, Gutiérrez O, Hirst L S and Ghosh S 2018 *Physical Review E* **97** 1–7

[10] Riahinasab S T, Keshavarz A, Melton C N, Elbaradei A, Warren G I, Selinger R L B, Stokes B J and Hirst L S 2019 *Nature Communications* **10** 1–10

[11] Vats A, Banerjee V and Puri S 2021 *Soft Matter* **17** 2659–2674

[12] Lin Y, Daoudi A, Dubois F, Segovia-Mera A, Legrand C and Douali R 2017 *Journal of Molecular Liquids* **232** 123–129

[13] Denolf K, Cordoyiannis G, Glorieux C and Thoen J 2007 *Physical Review E* **76** 051702

[14] Segura-Fernández F G, Serrato-García E F, Flores-Calderón J E and Guzmán O 2021 *Front. Phys.* `https://doi.org/10.3389/fphy.2021.636288`

[15] Anderson V, Terentjev E, Meeker S, Crain J and Poon W 2001 *The European Physical Journal E* **4**(1) 11–20

[16] Elder K R, Morin B, Grant M and Desai R C 1991 *Physical Review B* **44**(13) 6673–6688

[17] Kyrou C, Kralj S, Panagopoulou M, Raptis Y, Nounesis G and Lelidis I 2018 *Physical Review E* **97** 042701

[18] Starzonek S, Rzoska S J, Drozd-Rzoska A, Czupryński K and Kralj S 2017 *Physical Review E* **96** 022705

[19] Rivera B O, van Westen T and Vlugt T J H 2016 *Molecular Physics* **114**(6)

[20] Jana P K, Lam J, Mangal R, Alava M J, Parveen N and Laurson L 2021 *Physical Chemistry Chemical Physics* **23** 8825–8835

[21] Anderson J A, Glaser J and Glotzer S C 2020 *Computational Materials Science* **173**

[22] Martyna G J, Tobias D J and Klein M L 1994 *The Journal of Chemical Physics* **101**(5)

[23] Tuckerman M E, Alejandre J, López-Rendón R, Jochim A L and Martyna G J 2006 *Journal of Physics A: Mathematical and General* **39**(19)

[24] Charykov N, Charykova M, Semenov K, Keskinov V, Kurilenko A, Shaimardanov Z and Shaimardanova B 2019 *Processes* **7**(3)

[25] Sandmann M and Würflinger A 1998 *Zeitschrift für Naturforschung A* **53** 787–792

[26] Kim S, Chen J, Cheng T, Gindulyte A, He J, He S, Li Q, Shoemaker B A, Thiessen P A, Yu B, Zaslavsky L, Zhang J and Bolton E E 2021 *Nucleic Acids Research* **49** D1388–D1395

[27] Faetti S and Palleschi V 1984 *The Journal of Chemical Physics* **81** 6254–6258

[28] de Mesquita O N 1998 *Brazilian Journal of Physics* **28** 00–00

[29] Palermo M F, Pizzirusso A, Muccioli L and Zannoni C 2013 *The Journal of Chemical Physics* **138** 204901

[30] Widom B 1963 *The Journal of Chemical Physics* **39** 2808–2812

[31] Bennett C H 1976 *Journal of Computational Physics* **22** 245–268

[32] Perego C, Giberti F and Parrinello M 2016 *The European Physical Journal Special Topics* **225** 1621–1628

[33] Moore S G and Wheeler D R 2011 *The Journal of Chemical Physics* **134**(11)

[34] Agarwal A, Wang H, Schütte C and Site L D 2014 *The Journal of Chemical Physics* **141**(3)